"Gold Standard" 2D/3D Registration of X-Ray to CT and MR Images

Dejan Tomaevič, Boštjan Likar, and Franjo Pernuš

University of Ljubljana, Faculty of Electrical Engineering,
Traška 25, 1000 Ljubljana, Slovenia
{dejan.tomazevic,bostjan.likar,franjo.pernus}@fe.uni-lj.si

Abstract. Validation of registration techniques needed for image-guided surgery is an important problem, which received little attention in the literature. In this paper we address the challenging problem of generation of a reliable gold standard for evaluating the accuracy of surgical 2D/3D registrations. We have devised a cadaveric lumbar spine phantom with fiducial markers and established highly accurate correspondence between 3D CT and MR images and 18 2D X-ray images. The expected target registration errors are in the order of 0.2 mm for CT to X-ray registration and in the order of 0.3 mm for MR to X-ray registration. As such, the gold standard images, which are available on request from the authors, are useful for testing 2D/3D registration methods in image guided surgery.

1 Introduction

In image-guided orthopedic surgery, 3D preoperative medical data, such as CT and MRI, are commonly used to plan, simulate, guide, or otherwise assist a surgeon in performing a medical procedure. The plan, specifying how tasks are to be performed during surgery, is developed in the coordinate system of preoperative images. To monitor and guide a surgical procedure, the preoperative image and plan need to be transformed into physical space, i.e. a patient-related coordinate system. The spatial transformation is obtained by acquiring intraoperative data and registering them to data extracted from preoperative images [1]. More recent and promising approaches to obtain the spatial transformation rely on intraoperative x-ray projections acquired with a calibrated x-ray device. The location and orientation of a structure in 3D CT or MR image with respect to the geometry of the x-ray device is determined by 2D/3D registration [2-7].

A necessary step, required before wide spread clinical use of any novel registration technique, is the evaluation and validation of the method. While several researchers have addressed the validation problem in the context of particular methods [2-7], very little formal research has been done in this area. One difficulty in evaluating a registration technique is the need for highly accurate gold standard. Because it is practically impossible to establish gold standard registration with real patient data, simulated data or phantoms have to be considered. In this paper, we report on the creation of a cadaveric lumbar spine phantom to which fiducial markers were attached. 3D CT and MR and 2D X-ray images were acquired and accurate gold standard rigid registration between 3D and 2D images was established by means of fiducial markers. The accuracy of gold standard registration was assessed by target registration error [8].

T. Dohi and R. Kikinis (Eds.): MICCAI 2002, LNCS 2489, pp. 461–468, 2002.

2 Phantom Creation

A cadaveric lumbar spine, comprised of vertebra L1-L5 with some soft tissue, of an 80 year-old female was placed into a plastic tube and tied with thin nylon strings (Fig. 1, top-left). The tube was filled with water to simulate soft tissue and, therefore, to obtain more realistic MR, CT, and X-ray images. Six fiducial markers were rigidly attached to the outside of plastic tube (Fig. 1, bottom-left). Each fiducial marker had two parts, a base that could be screwed to a rigid body and a replaceable marker. Different markers were used for MR and CT and X-ray imaging. Markers, containing a metal ball (1.5 mm in diameter) were used for CT and X-ray imaging, while markers with a spherical cavity (2 mm in diameter) filled with water solution of Dotarem contrast agent (Gothia) were used for MR.

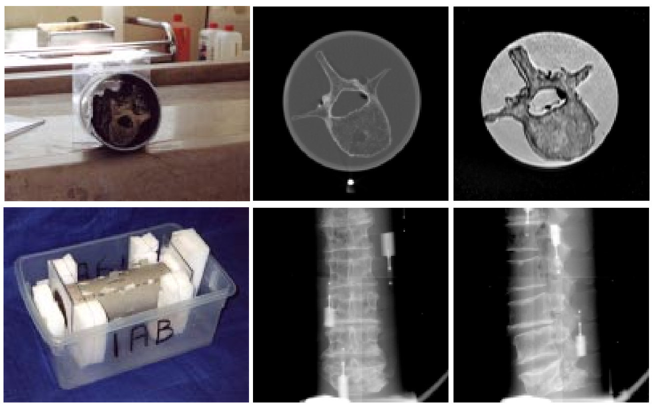

Fig. 1. The spine fastened in a plastic tube (top-left), final phantom with fiducial markers attached to the plastic tube (bottom- left), CT image (top-center), MR image (top-right), AP x-ray image (bottom-center), and lateral x-ray image (bottom-right) image.

3 Image Acquisition

The CT image (Fig. 1, top-center) was obtained with General Electric HiSpeed CT/i scanner at 100kV. Axial slices were taken with intra-slice resolution of 0.27x0.27 mm and 1 mm inter-slice distance. For MR imaging, Philips Gyroscan NT Intera 1.5 T scanner and T1 protocol was used (Fig. 1, top-right). Axial slices were obtained with 0.39x0.39 mm intra-slice resolution and 1.9 mm inter-slice distance. After acquisition, the acquired MR image was retrospectively corrected for intensity inhomogeneity by the information minimization method [9]. X-ray images (Fig. 1) were captured by PIXIUM 4600 (Trixell) digital X-ray detector. The detector had a 429x429 mm active surface, with 0.143x0.143 mm pixel size and 14-bit dynamic range. To simulate C-arm acquisition X-ray source and sensor plane were fixed while the spine phantom was rotated on a turntable (Fig. 2, left). In this way mechanical distortion due to gravitational force and other mechanical imperfections of C-arms were avoided, which resulted in a more precise acquisition. By rotating (step=20°) the spine phantom around its long axis, 18 X-ray images were acquired. The X-ray images were filtered by 3x3 median filter and then sub-sampled by the factor of two in order to remove dead pixel artifacts and to reduce the resolution.

4 Finding Centers of Fiducial Markers

In all 3D and 2D images a rough position $\mathbf{p}_m$ of each fiducial marker was first defined manually. Next, an intensity threshold I_T, that separated a marker from surrounding tissues, was selected for each marker. Finally, the center $\mathbf{p}_c$ of each marker was defined as:

$$\mathbf{p}_c = \frac{\sum_{\mathbf{p}\in\Omega}(I(\mathbf{p}) - I_T)\mathbf{p}}{\sum_{\mathbf{p}\in\Omega}(I(\mathbf{p}) - I_T)} \tag{1}$$

where $I(\mathbf{p})$ is the intensity at point $\mathbf{p}$ and Ω is a small neighborhood around point $\mathbf{p}_m$. By this method, centers of markers may be found to sub-pixel or sub-voxel accuracy. Let $\mathbf{X}_{MR}$ and $\mathbf{X}_{CT}$ be 3x6 matrices, each containing six 3D vectors representing the centers of fiducial markers found in MR and CT, respectively:

$$\begin{aligned}\mathbf{X}_{MR}&=[\mathbf{r}_1^{MR},\mathbf{r}_2^{MR},...,\mathbf{r}_6^{MR}]\\ \mathbf{X}_{CT}&=[\mathbf{r}_1^{CT},\mathbf{r}_2^{CT},...,\mathbf{r}_6^{CT}]\end{aligned} \tag{2}$$

where $\mathbf{r}=(x,y,z)^T$. Similarly, let $\mathbf{X}_\varphi$ be a 2x6 matrix involving six 2D points representing the centers of markers found in X-ray images obtained after rotating the phantom for φ degrees (φ=0°,20°,...,340°):

$$\mathbf{X}_\varphi=[\mathbf{p}_1^\varphi, \mathbf{p}_2^\varphi, ..., \mathbf{p}_6^\varphi] \tag{3}$$

where $\mathbf{p}=(x,y)^T$.

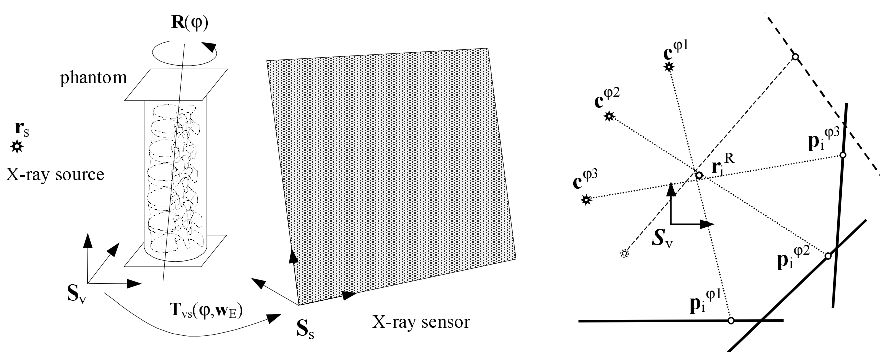

Fig. 2. X-ray image acquisition (left) and reconstruction of 3D marker position (right).

5 X-Ray Setup Calibration

The X-ray setup was calibrated retrospectively using the centers $\mathbf{X}_\varphi$ of fiducial markers found in X-ray images and the corresponding centers $\mathbf{X}_{CT}$ of markers found in CT volume. Calibration of the acquisition setup (Fig. 2) required the determination of the X-ray projection geometry and rotation between the coordinate system of the phantom and the coordinate system of the X-ray system. This involved determination of 12 geometrical parameters,3 intrinsic $\mathbf{w}_I$ and 9 extrinsic $\mathbf{w}_E$, denoted by calibration parameter vector $\mathbf{w}$, $\mathbf{w}=(\mathbf{w}_I^T,\mathbf{w}_E^T)^T$. The intrinsic parameters were describing the X-ray projection geometry while the extrinsic parameters were describing the rotation between the coordinate system of the phantom and the coordinate system of the X-ray setup.

The intrinsic parameters $\mathbf{w}_I=(x_s,y_s,z_s)^T$ define the position of the X-ray source $\mathbf{r}_s$ in the coordinate systems $\boldsymbol{S}_s$ of the sensor plane and, therefore, define the projection $\mathbf{P}_S(\mathbf{w}_I)$ of any 3D point described in the sensor coordinate system $\boldsymbol{S}_s$ to the 2D sensor plane. There are nine extrinsic parameters $\mathbf{w}_E$ needed to describe the rotation between the phantom and the X-ray system. Four parameters define the axis of rotation in coordinate system $\boldsymbol{S}_v$ of the phantom. We have chosen the coordinate system of the CT volume for $\boldsymbol{S}_v$. The axis of rotation is defined by point (tx_v,ty_v), which is the intersection of the axis with x-y coordinate plane of $\boldsymbol{S}_v$ and by rotation angles $(\omega x_v,\omega y_v)$ of the axis around x and y of $\boldsymbol{S}_v$. Similarly, four parameters (tx_s,ty_s) and $(\omega x_s,\omega y_s)$ define the same axis of rotation in coordinate system $\boldsymbol{S}_s$ of the X-ray sensor plane. The additional parameter, needed to determine the relation between $\boldsymbol{S}_s$ and $\boldsymbol{S}_v$ on the rotation axis, is distance d_{vs} between the two points of intersection (tx_v,ty_v) and (tx_s,ty_s). The extrinsic parameters $\mathbf{w}_E=(tx_v,ty_v,\omega x_v,\omega y_v,d_{vs},tx_s,ty_s,\omega x_s,\omega y_s)^T$ define transformation $\mathbf{T}_{VS}(\varphi,\mathbf{w}_E)$ that maps, for a given rotation φ of the phantom, any 3D point in coordinate system $\boldsymbol{S}_v$ to a 3D point in coordinate system $\boldsymbol{S}_s$:

$$\mathbf{T}_{VS}(\varphi,\mathbf{w}_E)=\mathbf{T}_{RS}(tx_s,ty_s,\omega x_s,\omega y_s)\cdot\mathbf{T}(d_{vs})\cdot\mathbf{R}(\varphi)\cdot\mathbf{T}_{VR}(tx_v,ty_v,\omega x_v,\omega y_v) \qquad (4)$$

where $\mathbf{T}_{VR}$ is the transformation from coordinate system $\boldsymbol{S}_v$ to the axis of rotation, $\mathbf{R}(\varphi)$ is the rotation around rotation axis, $\mathbf{T}(d_{vs})$ is the translation along rotation axis, and $\mathbf{T}_{RS}$ is the final transformation to the coordinate system $\boldsymbol{S}_s$. By merging projection $\mathbf{P}_S(\mathbf{w}_I)$ and transformation between the coordinate systems $\mathbf{T}_{VS}(\varphi,\mathbf{w}_E)$, the projection $\mathbf{P}_{VS}(\varphi,\mathbf{w})$ of 3D point defined in the coordinate system $\boldsymbol{S}_v$ to the 2D point lying in the sensor plane of $\boldsymbol{S}_s$ can be obtained for any rotation φ:

$$\mathbf{P}_{VS}(\varphi,\mathbf{w})=\mathbf{P}_S(\mathbf{w}_I)\mathbf{T}_{VS}(\varphi,\mathbf{w}_E) \qquad (5)$$

To calibrate the X-ray acquisition system, we thus need to define 12 geometrical parameters $\mathbf{w}$ of the projection $\mathbf{P}_{VS}(\varphi,\mathbf{w})$. The optimal calibration parameters $\mathbf{w}$ are the ones that bring the fiducial markers $\mathbf{X}_{CT}$ in CT volume to the best correspondence with the corresponding fiducial markers $\mathbf{X}_\varphi$ in X-ray images. To find the optimal parameters we project the centers of fiducial markers $\mathbf{X}_{CT}$ in CT volume to the sensor plane and compute the root mean squared (RMS) distance E_{calib} to the corresponding centers of fiducial markers $\mathbf{X}_\varphi$ in X-ray images:

$$E_{calib}(\mathbf{w})=\sqrt{\frac{1}{M}\sum_{\varphi\in\Phi}\frac{1}{N}\sum_{i=1}^{N}\left(\mathbf{p}_i^{\varphi}-\mathbf{P}_{VS}(\varphi,\mathbf{w})\,\mathbf{r}_i^{CT}\right)^2} \qquad (6)$$

where N and M stands for the number of fiducial markers and X-ray images, respectively, and $\Phi=\{\varphi_1,\varphi_2,\ldots,\varphi_M\}$ defines the X-ray images taken at different phantom rotations. To find the optimal calibration parameters $\mathbf{w}$, we used nine X-ray images $\Phi=\{0°,40°,...,320°\}$ and iterative optimization, which resulted in minimum RMS distance (E_{calib}) of 0.31 mm. The small RMS indicates that calibration was performed well and reflects the uncertainty of fiducial marker localization in CT and X-ray images.

6 Reconstruction of 3D Markers from Calibrated X-Ray Images

Once the X-ray acquisition system was calibrated, the positions of X-ray fiducial markers in 3D could be reconstructed from 2D X-ray images. Each point $\mathbf{p}_i^{\varphi}$, representing the center of i^{th} fiducial marker in X-ray image taken at rotation φ, was back-projected to the X-ray source $\mathbf{r}_s$, which yielded the projection line L_i^{φ} (Fig. 2, right). Line L_i^{φ} defines the perspective projection of a 3D marker to the 2D X-ray plane. The projection line L_i^{φ} can be expressed in the coordinate system $\boldsymbol{S}_v$ of the phantom by mapping the X-ray source $\mathbf{r}_s$ to point $\mathbf{c}^{\varphi}$:

$$\mathbf{c}^{\varphi} = \mathbf{T}_{\mathrm{VS}}^{-1}(\varphi, \mathbf{w}_{\mathrm{E}})\,\mathbf{r}_{\mathrm{s}} \tag{7}$$

and by expressing the line direction in $\boldsymbol{S}_v$ as:

$$\mathbf{v}_{\mathrm{i}}^{\varphi} = \frac{\mathbf{T}_{\mathrm{VS}}^{-1}(\varphi, \mathbf{w}_{\mathrm{E}})\,(\mathbf{p}_{\mathrm{i}}^{\varphi} - \mathbf{r}_{\mathrm{s}})}{\left|\mathbf{T}_{\mathrm{VS}}^{-1}(\varphi, \mathbf{w}_{\mathrm{E}})\,(\mathbf{p}_{\mathrm{i}}^{\varphi} - \mathbf{r}_{\mathrm{s}})\right|} \tag{8}$$

where $\mathbf{r}_s$ and $\mathbf{p}_i^{\varphi}$ are points defined in the sensor coordinate system $\boldsymbol{S}_s$.

We reconstructed a 3D marker position from X-ray images by finding the position of point $\mathbf{r}_i^R$ in the coordinate system $\boldsymbol{S}_v$ that minimized RMS distance E_{rec} from point $\mathbf{r}_i^R$ to all lines L_i^{φ}. E_{rec} can be expressed by vector products:

$$E_{rec}(\mathbf{r}_{\mathrm{i}}^{\mathrm{R}}) = \sqrt{\frac{1}{M}\sum_{\varphi\in\Phi}\left|(\mathbf{r}_{\mathrm{i}}^{\mathrm{R}} - \mathbf{c}^{\varphi}) \times \mathbf{v}_{\mathrm{i}}^{\varphi}\right|^2} \tag{9}$$

Reconstruction of 3D position of six fiducial markers from the nine X-ray images Φ={20°,60°,...,340°), which were not used for calibration, by iterative minimization of E_{rec} yielded RMS of less than 0.06 mm for each of the six fiducial markers. The reconstructed fiducial markers from X-ray images were incorporated in a 3x6 matrix $\mathbf{X}_R=[\mathbf{r}_1^R,\mathbf{r}_2^R,...,\mathbf{r}_6^R]$.

By using different sets of X-ray images for reconstruction and calibration, we were able to validate the calibration procedure. Small RMS of 0.06 mm indicated that the uncertainty of fiducial marker localization in X-ray images was smaller than in CT images and that calibration had been performed well. Therefore, the major source of calibration uncertainty is the uncertainty of fiducial marker localization in CT images, however, its effect on calibration precision is obviously very small.

7 Gold Standard Registration

After calibrating the X-ray acquisition system and reconstructing 3D markers $\mathbf{X}_R$ from X-ray images, we were able to establish gold standard registration between the X-ray and CT images, and between X-ray and MR images in coordinate system $\boldsymbol{S}_v$ of the phantom. This was achieved by rigid 3D/3D transformation $\mathbf{T}$ that minimized the RMS distance E_{reg} between reconstructed fiducial markers $\mathbf{X}_R$ from X-ray images and marker points $\mathbf{X}_{CT}$ from CT or $\mathbf{X}_{MR}$ from MR images:

$$E_{reg}(\mathbf{T}) = \sqrt{\frac{1}{N}\sum_{\mathrm{i}=1}^{N}\left(\mathbf{r}_{\mathrm{i}}^{\mathrm{R}} - \mathbf{T}\,\mathbf{r}_{\mathrm{i}}\right)^2} \tag{10}$$

where $\mathbf{r}_i$ stands for points $\mathbf{r}_i^{CT}$ or $\mathbf{r}_i^{MR}$. The closed form solution of this minimal RMS problem is known [8]. Rigid transformation $\mathbf{T}$ can be decomposed to the rotation component $\mathbf{R}$, represented by 4x4 matrix, and translation vector $\mathbf{t}$:

$$\mathbf{Tr} = \mathbf{Rr} + \mathbf{t} \tag{11}$$

The optimal solution for the translation component is given as:

$$\mathbf{t} = \overline{\mathbf{r}}^{R} - \mathbf{R}\overline{\mathbf{r}} \tag{12}$$

where $\overline{\mathbf{r}}^{R}$ and $\overline{\mathbf{r}}$ stand for mean position of point sets $\mathbf{X}_R$ and $\mathbf{X}$, respectively, and where set $\mathbf{X}$ can either be $\mathbf{X}_{CT}$ or $\mathbf{X}_{MR}$. The optimal solution for the rotation component is given as:

$$\mathbf{R} = \mathbf{BA}^{T} \tag{13}$$

A and **B** are two orthogonal matrices obtained by singular value decomposition (SVD) of the matrix:

$$\overline{\mathbf{X}}_{R}\overline{\mathbf{X}}^{T} = \mathbf{ADB}^{T} \tag{14}$$

where $\mathbf{D}$ is a diagonal matrix and $\overline{\mathbf{X}}_R$ and $\overline{\mathbf{X}}$ are the point sets $\mathbf{X}_R$ and $\mathbf{X}$, centered at corresponding mean positions $\overline{\mathbf{r}}^{R}$ and $\overline{\mathbf{r}}$, respectively.

Rigid registration of point set ($\mathbf{X}_{CT}$,$\mathbf{X}_R$) and ($\mathbf{X}_{MR}$,$\mathbf{X}_R$) resulted in minimum RMS distance E_{reg} of 0.27 mm for CT and 0.44 mm for MR to X-ray registration. Higher RMS for MR than for CT can be attributed to three reasons. First, because CT was used in calibration, second, because intra- and inter-slice resolution of MR images was lower than in CT, which resulted in higher fiducial localization uncertainty, and third, because MR images suffer from non-rigid spatial distortion.

8 Gold Standard Validation

The minimum RMS distance E_{reg} is also known as fiducial registration error FRE and can be used to evaluate the accuracy of point based rigid registration [8]. By knowing FRE we can determine target registration error (TRE), which is the distance between true, but unknown position of the target, and target position obtained by registration. The expected TRE of a target point $\mathbf{r}$ can be estimated from FRE [8]:

$$\left\langle TRE^2(\mathbf{r})\right\rangle = \frac{\left\langle FLE^2\right\rangle}{N}\left(1+\sum_{k=1}^{3}\frac{d_k}{f_k}\right) \tag{15}$$

where f_k is the RMS of the projections of fiducial markers to k^{th} principle axis of marker configuration, d_k is the projection of target point $\mathbf{r}$ to principle axis k, N is the number of fiducial markers, and FLE is the fiducial localization error obtained from FRE:

$$FLE^2 = \frac{N}{N-2}FRE^2 \tag{16}$$

Using the above formulation, we had validated the gold standard registration by manually defining eight target points, four per each pedicle (Fig. 3), in each of the 5 vertebra and computing mean TRE for each vertebra. The results of gold standard validation for CT to X-ray and MR to X-ray registration are illustrated in Table 1. The expected target registration errors for the pedicles are in the order of 0.2 mm for CT to X-ray registration and in the order of 0.3 mm for MR to X-ray registration.

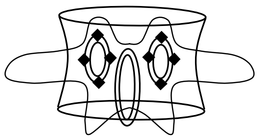

Fig. 3. The position of eight target points (◆) on the pedicle borders.

	Vertebrae				
	L1	L2	L3	L4	L5
CT	0.2	0.1	0.1	0.1	0.2
M	0.3	0.2	0.2	0.3	0.4

Table 1. The expected RMS TREs for gold standard registration in mm.

9 Discussion and Conclusion

We have devised a lumbar spine phantom and obtained and validated a gold standard rigid 2D/3D registration with the aim of testing the performances of methods for 2D/3D registration of X-ray to CT and MR images. Phantom data was composed of CT and MR volumes of the lumbar spine and a set of 18 X-ray projection images. X-ray images were obtained by rotating the phantom with a step of 20° around its principal axis, which mimics the intraoperative acquisition with C-arm. As such the phantom is useful for testing 2D/3D registration methods devised for intraoperative image guided surgery.

The X-ray acquisition system was calibrated retrospectively by matching the projections of CT markers with the corresponding markers in X-ray images. Calibration with CT markers is generally superior than calibration with MR markers because CT offers better resolution and spatial stability. This observation was confirmed experimentally, as CT-based calibration yielded smaller calibration error E_{calib} of 0.31 mm over 0.47 mm found with MR-based calibration. CT-based calibration of the X-ray image acquisition setup already provides registration of CT to X-ray images but does not give any indices of the registration accuracy.

We have consequently reconstructed the 3D positions of markers from calibrated 2D X-ray images, which allowed us to implement 3D/3D registration between the reconstructed markers and those found in CT and MR volumes. The result of such a registration reflects: a) uncertainty of marker localization in 2D X-ray images, b) uncertainty of marker localization in 3D CT or MR images, c) uncertainty of the X-ray acquisition calibration, and d) uncertainty of marker reconstruction. Altogether, the uncertainties caused fiducial registration error (FRE) of 3D/3D registration, which was used to evaluate target registration error (TRE) of the gold standard CT to X-ray and MR to X-ray registration by the theory developed in [8].

The results in Table 1 indicate that gold standard registration is highly accurate and therefore useful for testing 2D/3D registration methods. However, it should be stressed that the expected TREs for CT to X-ray gold standard registration may possibly be a little larger than those presented in Table 1. This is because the same CT markers were used for X-ray system calibration and for CT to X-ray registration, which could had involved the same bias in the calibration and registration. Nevertheless, if we assume that localization errors for CT markers are much smaller than for MR markers, the expected TREs for CT to X-ray gold standard registration should be close to those given in Table 1 and are certainly not larger than TREs for MR to X-ray registration.

The gold standard image data is available on request from the authors, who believe it will prove useful for validation of newly developed methods with the same data and therefore provide comparison among different registration methods, especially due to the lack of publicly available gold standards for 2D/3D registration.

Acknowledgements

The authors would like to thank Laurent Desbat, Markus Fleute and Raphael Martin, University Joseph Fourier, Grenoble, France, Francois Eesteve of Rayonnement Synchrotron et Recherche Medicale, Grenoble, France, and Uroš Vovk of University of Ljubljana for their generous help and support in acquisition of images. This work was supported by the IST-1999-12338 project, funded by the European Commission and by the Ministry of Education, Science and Sport, Republic of Slovenia.

References

1. R. L. Galloway, "The process and development of image-guided procedures," *Annual Rev. Biomed. Eng.*, vol. 3, pp. 83-108, 2001.
2. S. Lavallée and R. Szeliski, "Recovering the position and orientation of free-form objects from image contours using 3D distance maps," *IEEE Transaction on Pattern Analysis Machine Intelligence*, vol. 17, pp. 378-390, 1995.
3. Guéziec, P. Kazanzides, B. Williamson and R. H. Taylor, "Anatomy-based registration of CT-scan and intraoperative X-ray images for guiding a surgical robot," *IEEE Transaction on Medical Imaging*, vol. 17, pp. 715-728, 1998.
4. L. Lemieux, R. Jagoe, D. R. Fish, N. D. Kitchen, D. G. T. Thomas, "A patient-to-computed-tomography image registration method based on digitally reconstructed radiographs," *Medical Physics*, vol. 21, pp. 1749-1760, 1994.
5. J. Weese, G. P. Penny, P. Desmedt, T. M. Buzug, D. L. G. Hill, and D. J. Hawkes, " Voxel-Based 2-D/3-D Registration of Fluoroscopy Images and CT Scans for Image-Guided Surgery," *IEEE Transactions on Information Technology in Biomedicine*, vol. 1, pp. 284-293, 1997.
6. G. P. Penny, J. Weese, J. A. Little, P. Desmedt, D. L. G. Hill, and D. J. Hawkes, "A comparison of Similarity Measures for Use in 2-D-3-D Medical Image Registration," *IEEE Transactions on Medical Imaging*, vol. 17, pp. 586-595, 1998.
7. D. LaRose, J. Bayouth, and T. Kanade, "Transgraph: interactive intensity-based 2D/3D registration of X-ray and CT data", *Medical Imaging 2000*, San Diego, USA, K. M. Hanson (ed), SPIE Press 3979:385-396 (2000).
8. J. M. Fitzpatrick, J. B. West, and C. R. Maurer, "Predicting Error in Rigid-Body Point-Based Registration," *IEEE Transactions on Medical Imaging*, vol. 17, pp. 694-702, 1998.
9. B. Likar, M. A. Viergever, and F. Pernuš, "Retrospective correction of MR intensity inhomogeneity by information minimization", *IEEE Transactions on Medical Imaging*, vol. 20, pp. 1398-1410, 2001.